

The Effect of the Detector Response Time on Bolometric Cosmic Microwave Background Anisotropy Experiments

S. Hanany,¹* A. H. Jaffe,¹† and E. Scannapieco^{1,2}‡

¹ The Center for Particle Astrophysics, University of California, Berkeley, 301 Le Conte Hall, Berkeley, CA, 94720-7304.

² Physics Department, University of California, Berkeley, CA 94720

26 February 2018

ABSTRACT

We analyze the effects of the detector response time on bolometric measurements of the anisotropy of the cosmic microwave background (CMB). We quantify the effect in terms of a single dimensionless parameter L defined as the ratio between the time the beam sweeps its own size and the bolometer response time. As L decreases below ~ 2.5 the point source response of the experiment becomes elongated. We introduce a window function matrix based on the timestream data to assess the effects of the elongated beam. We find that the values of the window function matrix elements decrease slowly as a function L . Our analysis and results apply to other cases of beam asymmetry. For the High Frequency Instrument on board the Planck Surveyor satellite we show that for a broad range of L the ability of the experiment to extract the cosmological parameters is not degraded. Our analysis enhances the flexibility in tuning the design parameters of CMB anisotropy experiments.

Key words: cosmic microwave background – methods: data analysis – methods: observational

1 INTRODUCTION

The anisotropy of the cosmic microwave background (CMB) radiation encodes a vast amount of information about structure formation in the universe and about the values of the cosmological parameters (White, Scott & Silk 1994). A number of groups are now making efforts to map the CMB at resolutions of 10–20 arcmin. Two satellite missions, NASA’s MAP and ESA’s Planck Surveyor, are scheduled to be launched within the next decade.

In a substantial fraction of ongoing and planned experiments the detector elements are bolometers. Bolometers are thermal detectors and thus have a response time that depends on a variety of construction and operation parameters (Richards 1994). Time constants of bolometers currently employed on CMB experiments are on the order of 10 msec. The baseline design for Planck’s High Frequency Instrument (HFI) bolometers is between 2 and 5 msec.

The bolometer response time puts a practical constraint on the speed with which a bolometric experiment can scan the sky. Scanning too fast decreases the sensitivity of the experiment to structures near the beam resolution. On the

other hand, the scan speed and the detector’s $1/f$ noise knee determine the number of time-ordered pixels over which the noise is uncorrelated. A faster scan speed allows a more robust characterization of the instrumental noise and better recovery of the sky signal over a larger angular range (Tegmark 1997a; Tegmark 1997b). Thus there are important trade-offs between the detector noise level, time constant, beam size and scan speed that must be considered when optimizing the experiment. In the case of the Planck Surveyor instruments, for example, a balance has to be found between the requirements of the low frequency HEMT-based instrument (LFI) and the bolometric high frequency instrument. The LFI prefers a fast scan speed because both its detector response speed and $1/f$ noise knee are higher than for the HFI. However, if the scan speed is too fast HFI’s performance at high resolution will degrade.

The window function matrix, and its trace, the window function, quantify the sensitivity of a CMB anisotropy experiment as a function of angular scale. The full matrix contains information about all possible pixel pairs; the simpler window function, W_ℓ , reduces this to the RMS anisotropy probed by the experiment. A number of authors have analyzed how the beam size and scan strategy determine the window function (see White et al. (1994) and references therein). It has traditionally been assumed that the bolometer response time can be neglected. With a window function at hand, algorithms have been developed to asses the accu-

* hanany@physics.berkeley.edu

† jaffe@physics.berkeley.edu

‡ evan@physics.berkeley.edu

racy with which a given experiment can extract the cosmological parameters (Jungman et al. 1995; Bond, Efstathiou & Tegmark 1997; Zaldarriaga, Spergel & Seljak 1997). All of these calculations assume that the experiment illuminates the sky with a symmetric beam and that the noise in the experiment is uncorrelated, and hence that off-diagonal elements of the window function matrix are unimportant.

In this paper we analyze how the window function matrix of a bolometric experiment depends on the combination of bolometer response time, beam size, and scan speed. When the detector response time cannot be neglected, the effective shape of the beam becomes elongated and the form of the window function matrix becomes a complicated function of the scan strategy and pixelization. Furthermore, the standard techniques used to assess the accuracy with which a given experiment can extract cosmological parameters from the data are no longer strictly valid since they assume that the beam is symmetric. We overcome the difficulties associated with constructing a window function matrix and assessing the performance of the experiment in the presence of an asymmetric beam by introducing a window function constructed from data points pixelized in the time domain. We use this ‘temporal’ window function matrix to evaluate the window function as a function of the detector response time and to estimate the magnitude of the necessary corrections to the off-diagonal elements. The discussion focuses on the potential reduction in the window function matrix response near the nominal resolution of the experiment. Our analysis and results will be applicable to any asymmetric beam elongation that decreases the nominal resolution in one direction. As a special application, we calculate the ability of Planck-HFI to extract cosmological information as a function of different values of the instrumental parameters.

In Section 2 we derive the effect of the detector response time on the point source response of the experiment. We then derive the necessary changes to the zero lag window function (Sections 3.1, 3.2) and assess Planck-HFI’s performance (Section 3.3). In Section 3.4 we concentrate on the full window function matrix in the presence of the beam asymmetry introduced by the detector response time. We discuss and summarize the results in Section 4.

2 BOLOMETER TIME CONSTANT AND POINT SOURCE RESPONSE

A bolometer is a thermal detector in which absorbed radiation is converted to heat, causing a temperature change that is proportional to the absorbed energy. A thermistor is used to measure the temperature change. The temporal response of bolometers is an exponential; if the bolometer temperature is T_0 at time $t < 0$, then upon a step function increase in input power at time $t = 0$,

$$T(t > 0) = T_0 + \Delta T(1 - \exp(-t/\tau)). \quad (1)$$

The time constant τ depends on the heat capacity of the absorbing medium, on the detector’s thermal conductivity to its mounting structure, and on properties of the thermistor (Richards 1994). The exponential response time τ is a single-pole low-pass filter in the frequency response of a bolometric experiment. The filter is given by

$$F(\omega) = \frac{1 - i\omega\tau}{1 + (\omega\tau)^2}. \quad (2)$$

The amplitude response of the filter has a -3 dB point[§] at a frequency $f_{\text{bolo}} = 1/(2\pi\tau)$.

In an observing strategy where the optical beam is scanned across the sky the bolometer time constant can be viewed as a single-pole low pass filter in the spatial domain. Since all of the effects we will be discussing are relevant only at small angular scales, we approximate the region of interest on the sky as flat and use Fourier transforms on the plane. If we write $\omega = \mathbf{k} \cdot \mathbf{v}$, where \mathbf{k} is the spatial wavenumber being probed, and \mathbf{v} is the angular velocity of the pointing on the sky, we get for the response in \mathbf{k} -space

$$F(k) = \frac{1 - ikv\tau \cos \theta_{kv}}{1 + (kv\tau \cos \theta_{kv})^2} \quad (3)$$

where θ_{kv} is the angle between the vectors \mathbf{k} and \mathbf{v} . F is a complex filter. Its amplitude response is

$$|F(k)| = \frac{1}{\sqrt{1 + (kv\tau)^2 \cos^2 \theta_{kv}}}, \quad (4)$$

and its phase is

$$\phi = \tan^{-1}(-kv\tau \cos \theta_{kv}). \quad (5)$$

The amplitude response of the filter has a -3 dB point at $k_{3dB} = 1/(v\tau \cos \theta_{kv})$ which depends on the instantaneous scan speed v . From now on we will implicitly assume that, where relevant, the scan speed is constant. The approximation of a flat sky is valid for regions smaller than $\sim 20 \times 20$ deg². Within this approximation $k \simeq \ell$, where ℓ is the multipole number of the $Y_{\ell m}$ spherical harmonics.

Assume that the optical system of a bolometric experiment produces a symmetric beam $B(\mathbf{r}, \sigma)$, where σ is a measure of the size of the beam (e.g., the width of a Gaussian beam), and \mathbf{r} locates it. The position \mathbf{r} is defined relative to coordinates located on the region of interest on the sky. If the beam is swept across the sky at a constant velocity \mathbf{v} the point source response is the convolution of the beam and the temporal response of the detector:

$$S(\mathbf{r}, \mathbf{v}, \tau, \sigma) = \int B(|\mathbf{r} - \mathbf{r}'|, \sigma) F(\mathbf{r}', \mathbf{v}, \tau) d^2 \mathbf{r}'; \quad (6)$$

equivalently,

$$S(\mathbf{r}, \mathbf{v}, \tau, \sigma) = \int \exp(-i\mathbf{k} \cdot \mathbf{r}) B(\mathbf{k}, \sigma) F(\mathbf{k}, \mathbf{v}, \tau) \frac{d^2 \mathbf{k}}{(2\pi)^2}, \quad (7)$$

where, to simplify notation, we use $B(\mathbf{k})$ and $F(\mathbf{k})$ as the Fourier transforms of $B(\mathbf{r})$ and $F(\mathbf{r})$. Since $F(k)$ is complex, the resulting response S is both attenuated and phase shifted compared to the case $\tau = 0$. A dimensionless figure of merit that quantifies the level of attenuation and phase shift is L , defined as

$$L \equiv \frac{\sigma}{v\tau} = \frac{\sigma/v}{\tau} = \frac{f_{\text{bolo}}}{f_{\text{scan}}}. \quad (8)$$

Since σ/v is the time it takes the beam to cross a distance equal to its width, $L \gg 1$ corresponds to the case where the time constant is short compared to this crossing time and spatial filtering is negligible. $L \ll 1$ corresponds to the case

[§] dB = $20 \log_{10}(|F|)$

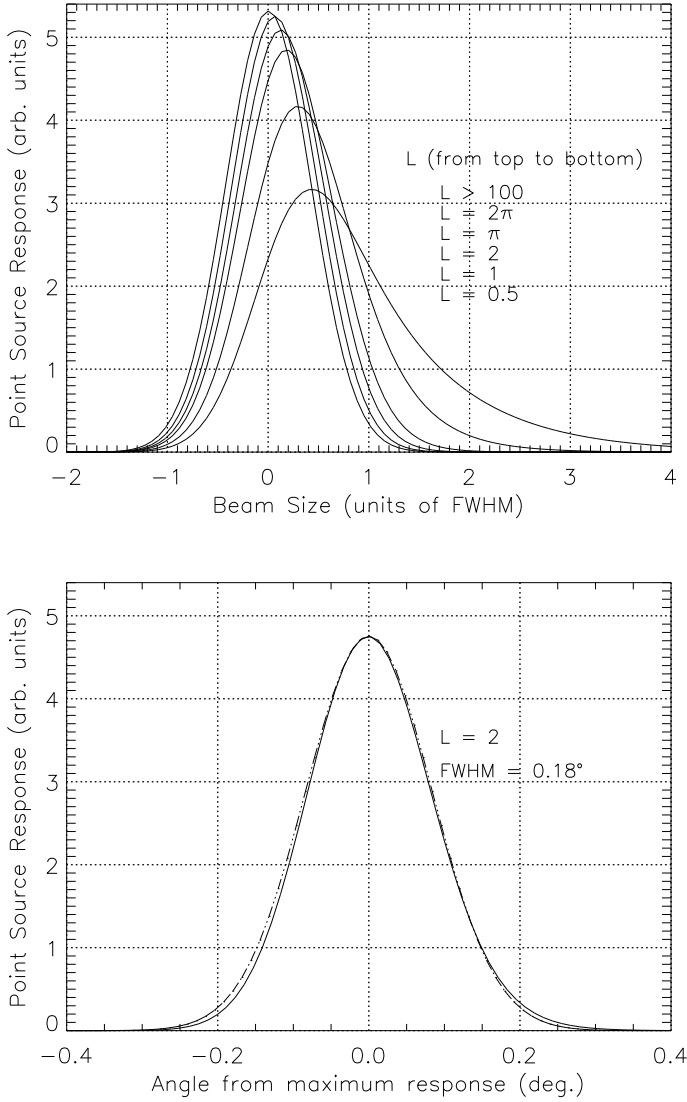


Figure 1. Top panel: The point source response of a Gaussian beam as a function of $L = \sigma/(v\tau)$, where σ is the width the beam, v is the scan speed, and τ is the bolometer time constant. For $L \gg 1$ there is little change in the shape of the beam. For $L \leq 2$ the point source response is phase shifted and attenuated. Bottom panel: For values of $L > 2$ the effective shape of the beam in the direction of the scan is well approximated by a Gaussian with a width $\sigma_{1d}^2 \simeq \sigma^2 + (v\tau)^2$. Shown are the effective shape (full curve) and the Gaussian fit (dash-dot) for $L = 2$.

where the time constant is much slower than the crossing time and spatial filtering is expected to be significant. In the frequency (1/time) domain, L is the ratio between the bolometer time constant low-pass filter f_{bolo} and the width of the point source response with $\tau = 0$, $f_{\text{scan}} \equiv v/(2\pi\sigma)$ (Hristov 1994). For a Gaussian beam f_{scan} is at the $1/e$ point of the point source response.

The upper panel in Figure 1 shows the point source response of an initially Gaussian beam for a range of L values. For a nominal two-dimensional Gaussian beam,

$$B(\mathbf{r}, \sigma) = \frac{1}{2\pi\sigma^2} e^{-r^2/(2\sigma^2)} \quad (9)$$

and

$$B(\mathbf{k}, \sigma) = e^{-k^2\sigma^2/2}. \quad (10)$$

As expected, small values of L result in a larger effective beam in the direction of the scan. The shape in a direction perpendicular to the scan direction is not affected. Overall, the larger effective beam size will result in a degraded sensitivity to spatial structures which are on the scale of the nominal resolution.

For values of $L \gtrsim 2$ the spatial filter (Eq. 4) can be approximated as a Gaussian. When combined with a nominal Gaussian beam of width σ the Fourier transform, Eq. 7, can be solved exactly, and one finds that the effective beam in the direction of the scan has acquired an additional Gaussian of width $\sigma_{\text{bolo}}^2 \simeq (v\tau)^2$. The total beam width in the direction of the scan is now

$$\sigma_{1d}^2 \simeq \sigma^2 + (v\tau)^2 = \sigma^2(1 + L^{-2}). \quad (11)$$

The lower panel of Fig. 1 shows the effective beam shape and the Gaussian that approximates it for $L = 2$. The resulting 2-dimensional beam is elliptical with a width σ_{1d} in the direction of the scan and σ in a direction perpendicular to the scan.

3 WINDOW FUNCTION AND COSMOLOGICAL PARAMETER ESTIMATION

We now quantify the effect of the enlarged asymmetric beam on the window function of the experiment and its effect on the estimation of cosmological parameters. We ignore the spatial phase shifts of the signal. In most real situations the phase shift will either be small compared to the beam size or the need to accurately reconstruct the beam location (for e.g., making an accurate map) will force experimenters to determine and correct for it.

3.1 Temporal Window Function

We begin with the temporal data stream which consists of data labeled by both position on the sky and time. The signal at a given time $t = 1 \dots N_t$ is a convolution of the beam pattern with the underlying sky signal:

$$s_t = \int d^2\hat{\mathbf{x}} \mathcal{F}_t(\hat{\mathbf{x}}) \frac{\Delta T}{T}(\hat{\mathbf{x}}) = \sum_{\ell m} \mathcal{F}_{t\ell m} a_{\ell m} \quad (12)$$

where we have transformed to spherical harmonics in the second equality. The kernel \mathcal{F} encodes the beam shape and its location on the sky at time t . If we consider small areas of sky, on which the time-constant effects will be relevant, we can again consider the sky to be flat and approximate the spherical harmonics with Fourier transforms. Then the signal is

$$s_t = \int \frac{d^2\mathbf{k}}{(2\pi)^2} a(\mathbf{k}) \mathcal{F}_t(\mathbf{k}), \quad (13)$$

with

$$\langle a(\mathbf{k}) a(\mathbf{k}') \rangle = (2\pi)^2 \delta^2(\mathbf{k} + \mathbf{k}') C(k), \quad (14)$$

and

$$C_\ell \simeq C(k)|_{\ell \simeq k}. \quad (15)$$

The temporal signal correlation matrix is

$$S_{tt'} = \langle s_t s_{t'} \rangle = \int d\ln k W_{tt'}(k) \frac{k^2 C(k)}{2\pi} \quad (16)$$

with the temporal window function matrix

$$W_{tt'}(k) = \int \frac{d\theta_k}{2\pi} e^{-ikr_{tt'} \cos \theta_k} U_{tt'}(\mathbf{k}) B^2(k) \quad (17)$$

where we have split off the effect of a symmetric beam $B(k)$ and other asymmetric parts U . Here, $r_{tt'}$ is the angular distance between pixels observed at times t, t' . An experiment with $U = 1$, (i.e., a symmetric beam, and no chopping), has

$$W_{tt'}(k) = J_0(kr_{tt'}) B^2(k). \quad (18)$$

For $t = t'$ we get the zero-lag window function

$$W_{tt}(k) = B^2(k). \quad (19)$$

With the spatial asymmetry of the beam, induced by the bolometer time constant (Eq. 4), the temporal window function matrix becomes

$$\begin{aligned} W_{tt'}(k) &= B^2(k) \int \frac{d\theta_k}{2\pi} e^{-ikr_{tt'} \cos \theta_k} \\ &\times [1 + (kv\tau)^2 \cos^2(\theta_k - \theta_t)]^{-1/2} \\ &\times [1 + (kv\tau)^2 \cos^2(\theta_k - \theta_{t'})]^{-1/2}, \end{aligned} \quad (20)$$

where $\theta_t, \theta_{t'}$ are the angles of the velocity vector \mathbf{v} at times t and t' .

3.2 Zero Lag Window Function

To obtain the traditional window function of the experiment, which encodes contributions only to the RMS signal, we set $t = t'$ in Eq. 20, giving

$$\begin{aligned} W_{tt}(k) &= B^2(k) \int \frac{d\theta_k}{2\pi} [1 + (kv\tau)^2 \cos^2(\theta_k - \theta_t)]^{-1} \\ &= B^2(k) \frac{1}{\sqrt{1 + (k/k_\tau)^2}} \end{aligned} \quad (21)$$

where

$$k_\tau \simeq \ell_\tau \equiv \frac{1}{v\tau} = \frac{1.8 \cdot 10^5}{\pi} \left(\frac{1\text{ms}}{\tau} \right) \left(\frac{1\text{deg/sec}}{v} \right). \quad (22)$$

The original window function, which was composed of the beam spatial filter, $W_{\tau=0}(k) = B^2(k)$, is now multiplied by an additional single-pole low-pass filter,

$$\begin{aligned} R(\ell) &\simeq R(k) = W(k)/W_{\tau=0}(k) \\ &= [1 + (k/k_\tau)^2]^{-1/2} \simeq [1 + (\ell/\ell_\tau)^2]^{-1/2}. \end{aligned} \quad (23)$$

The -3 dB point of $R(\ell)$ is at $\ell = \ell_\tau$. The beam filter has a low-pass cut-off at $\ell_\sigma \equiv 1/\sigma$. The shape of the filter depends on the shape of the beam. (A Gaussian beam with width σ has an exponential low pass $B^2(k) = \exp(-\ell^2\sigma^2)$.) Thus the effects of beam elongation will be important when

$$\ell_\tau \leq \ell_\sigma \Rightarrow L = \frac{\ell_\tau}{\ell_\sigma} \lesssim 1. \quad (24)$$

Figure 2 shows the zero lag window function for an originally Gaussian symmetric beam and for various values of L .

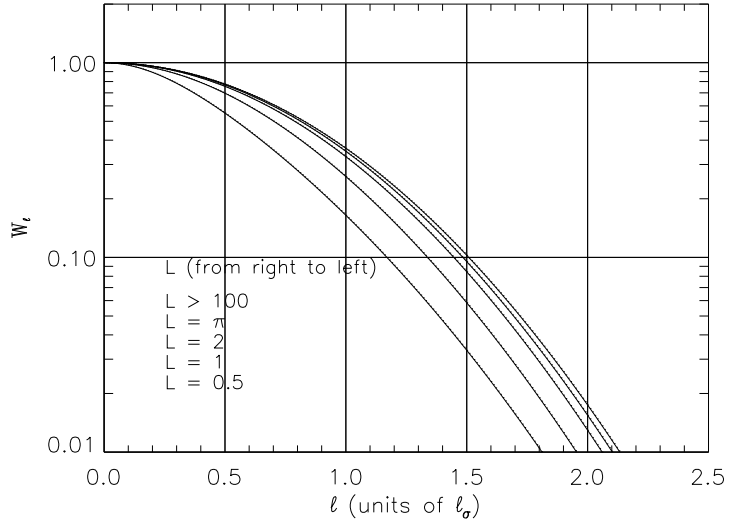


Figure 2. The zero lag window function, Eq. 21, with an initially Gaussian beam for a range of L values. The horizontal axis is in units of $\ell_\sigma = 1/\sigma$.

We point out that the window function calculated from the timestream, Eq. 21, is the *same* as the one calculated from a map,

$$W_\ell = \frac{1}{N_p} \sum_{N_p} W_{pp}(\ell), \quad (25)$$

where p denotes a pixel location on the sky. The window function, in any representation, just measures the sensitivity to the RMS temperature, and does not take into account pixel-pixel correlations.

For a reasonable range of v and $\tau, \ell_\tau \gtrsim 800$, below which most of the cosmological information resides in CDM-like models. For these cases, and for $\ell \lesssim \ell_\tau$, the single-pole filter R_ℓ can be usefully approximated by a Gaussian. By Taylor expanding $(1 + \ell^2/\ell_\tau^2)^{-1/2}$ and matching with the first term of a similar expansion for a Gaussian we find that

$$W_g(\ell) \simeq B^2(\ell) e^{-\ell^2\sigma'^2} = e^{-\ell^2(\sigma^2 + \sigma'^2)} \quad (26)$$

where

$$\sigma'^2 \equiv \frac{1}{2\ell_\tau^2} = \frac{(v\tau)^2}{2}, \quad (27)$$

and we have specialized to a Gaussian beam in the equality. This can be thought of as approximating the nearly ellipsoidal effective beam by a circular Gaussian beam with a slightly larger width. This new width,

$$\sigma_{2d}^2 \simeq \sigma^2 + \frac{(\ell_\tau)^2}{2} = \sigma^2(1 + L^{-2}/2) \quad (28)$$

is larger than the original width σ and smaller than the one dimensional effective width that we found in the previous section; see Eq. 11. That is, we find a degradation in the window function response compared to the original σ^2 width, but not as severe as indicated by the beam elongation in the scan direction, $\sigma_{1d}^2 = \sigma^2(1 + L^{-2})$. This is because beam elongation occurs primarily in one direction whereas the window function encodes information from all spatial

directions. Generally, as can also be observed by Comparing Figs. 1 and 2, the effects of small values of L are stronger in the spatial domain than they are on the window function.

The effective Gaussian filter $\exp(-\ell^2(\sigma^2 + \sigma'^2))$ is the geometric mean of two Gaussian filters corresponding to two symmetric beams (White 1997),

$$B^2(k) = \sqrt{B_\sigma^2(k)B_{\sigma_{1d}}^2(k)}. \quad (29)$$

One has a width σ_{1d} corresponding to the effective beam in the scan direction and the other has a width σ corresponding to the nominal beam size. The Gaussian approximation is good to within 10% for all ℓ less than $.88\ell_\tau$. As an example, $\ell_\tau = 1680$ for $\tau = 5$ msec. and $v = 6$ deg./sec. which are the time constant for Planck's 100 GHz bolometric channel, and the satellite rotation rate, respectively, and thus the approximation is valid for $\ell \leq 1480$.

3.3 Estimation of Cosmological Parameters

Given the window function $W(k)$ (Eq. 21), we use the apparatus that has been developed by Jungman et al. (1996) and others (Bond et al. 1997; Zaldarriaga et al. 1997) to estimate its effect on the determination of cosmological parameters. We specialize the discussion to the experimental configuration of the High Frequency Instrument (HFI) on board the Planck Surveyor satellite.

Each of the panels of Table 1 represents a different cosmological model. For each of the models we calculate the error in the determination of a variety of cosmological parameters for three values of the parameter L . $L_0 = 2.67$ is chosen to represent the value presently designed for the HFI instrument.

Within the bounds of validity of the analysis (see below), we find that for the case of the HFI choosing L values which are a factor of 2 or 5 smaller than the nominal L_0 would not significantly affect the ability to extract the values of the cosmological parameters. Note that the effect of the smearing is almost completely negligible for $L \gtrsim L_0/2 \simeq 1.33$ and begins to be noticeable with the three significant figures in the table at $L \simeq L_0/5 \simeq 0.5$. We defer a more detailed discussion of this result to Section 4.

The results in Table 1 should be read with some caution. The forecasts of parameter errors assume a form for the covariance matrix (more precisely, the Fisher Matrix; see Section 3.4.1) which is appropriate for an experiment with a symmetric beam and uniform, uncorrelated pixel errors. Since in our case the beam is manifestly not symmetric we expect these forecasts to be only approximate. Furthermore, our analysis considers quantities in the time domain. The relationship between pixel- and time-domain is not completely straightforward in the presence of beam asymmetry; this is a topic of current research. In the limit of many crossings through the same pixel in many different directions, the requirement for an effectively symmetric beam is satisfied, if we consider quantities in the pixel, rather than time, domain. In other cases it will not be satisfied and care must be taken in interpreting the results in Table 1. White (1997) has noted that it may be possible to get a pixel-domain window function that is narrower than the time stream window function that we use here by certain signal-to-noise weighting techniques. More generally, it has been noted that the

$h = 0.5$ SCDM	L_0	$L_0/2$	$L_0/5$
H_0 [rel]	0.021	0.021	0.024
Ω_0	0.002	0.002	0.002
Ω_{vac}	0.049	0.050	0.058
$\Omega_b h^2$ [rel]	0.006	0.006	0.007
Ω_ν	0.018	0.018	0.020
n	0.006	0.006	0.007
tensor/scalar	0.095	0.095	0.098
τ	0.155	0.155	0.158
<hr/>			
$\Omega = 0.33$, $h = 0.6$ open CDM	L_0	$L_0/2$	$L_0/5$
H_0 [rel]	0.011	0.011	0.015
Ω_0	0.001	0.001	0.001
Ω_{vac}	0.016	0.017	0.021
$\Omega_b h^2$ [rel]	0.008	0.008	0.009
n	0.003	0.003	0.003
τ	0.053	0.053	0.054
<hr/>			
$\Omega = 0.33$, $\Omega_\Lambda = 0.66$, $h = 0.7$ CDM	L_0	$L_0/2$	$L_0/5$
H_0 [rel]	0.011	0.011	0.013
Ω_0	0.002	0.002	0.002
Ω_{vac}	0.030	0.030	0.035
$\Omega_b h^2$ [rel]	0.007	0.007	0.008
n	0.007	0.007	0.007
tensor/scalar	0.078	0.078	0.080
τ	0.146	0.147	0.152

Table 1. The three columns of numbers quantify the accuracy with which the Planck Surveyor HFI will be able to determine a variety of cosmological parameters as a function of $L = \sigma/v\tau$, where σ is the width of a Gaussian beam, v is the scan speed, and τ is the detector time constant. The parameter $L_0 = 2.67$ is appropriate for the baseline design of the HFI. The calculation assumes 4 frequency channels at 100, 143, 217, 353 GHz, Gaussian beams with FWHM 10.6, 7.4, 4.9, 4.5 arcmin, nominal sensitivities of 4.9, 4.8, 9.7, $40\mu K/\text{pixel}$, respectively, and a scan rate of 6 deg./sec. The notation 'rel' is for fractional errors with respect to the model. Due to a degeneracy between Ω_{vac} and Ω_0 , we hold the curvature, $1 - \Omega_0 - \Omega_{\text{vac}} - \Omega_b - \Omega_\nu$, fixed for the error determination, except in the determination of Ω_0 itself, for which we fix Ω_{vac} .

least-squares method of Wright (1996), which is a variant of the method originally used to make the COBE/DMR maps (see also (Tegmark 1997a; Tegmark 1997b)), produces a map containing all of the sky information of the experiment. The method, as implemented in these references, assumes a known timestream noise matrix $N_{tt'}$ and uses it to estimate the temperature at a pixel p given measurements of the temperature at p taken at different times. With an asymmetric beam, individual measurements taken at p no longer measure quite the same quantity due to the differing beam orientations. This can be accounted for at the cost of greatly complicating the matrices used in the solution to the problem. Such a treatment is beyond the scope of this paper. For the results of Table 1 we used timestream quantities and the RMS window function $W(k)$. We will return to the question of beam asymmetry and assess its impact on the window function matrix, and on the ability to extract cosmological parameters, in the following section.

Finally, the standard analysis, which leads to the results

in Table 1, makes several additional assumptions that need to be highlighted. The actual likelihood as a function of the cosmological parameters will be highly non-Gaussian, but the calculations assume Gaussianity (at least near the peak of the distribution). In addition, the results assume that the removal of foregrounds and systematic effects proceeds without appreciable degradation of the satellite’s sensitivity.

3.4 Full Window Function Matrix

The analysis in terms of the zero-lag window function is an approximation that neglects pixel-pixel, or beam-beam correlations. We now assess whether sweeping an effectively asymmetric beam across the sky significantly affects this approximation. We first parameterize the relative power spectrum errors $\delta C_\ell/C_\ell$ in terms of the symmetric beam errors and a . The parameter a quantifies the ‘average’ ratio in the beam-beam correlations between the symmetric and asymmetric beam cases. We then assess the magnitude of a .

3.4.1 Off-Diagonal Elements and Parameter Estimation

The (ensemble average) error on the cosmological parameters b_i is given by

$$\langle \delta b_i \delta b_{i'} \rangle = F_{ii'}^{-1}, \quad (30)$$

where $F_{ii'}$ is the *Fisher Matrix* given by

$$F_{ii'} = \frac{1}{2} \text{Tr} \left(C^{-1} \frac{\partial C}{\partial b_i} C^{-1} \frac{\partial C}{\partial b_{i'}} \right). \quad (31)$$

Here $C = C_{pp'}$ is the total correlation matrix (in pixel space, although the arguments hold for the timestream data as well) of the data in question, which has contributions from both signal and noise: $C = C(S, N) = S + N$. In particular, the signal part of the matrix is given by

$$S_{pp'} = \sum_\ell \frac{2\ell + 1}{4\pi} W_{pp'}^\ell C_\ell. \quad (32)$$

Thus, if we parameterize by the power spectrum itself the derivatives are just

$$\frac{\partial C}{\partial C_\ell} = \frac{\partial S}{\partial C_\ell} = \frac{2\ell + 1}{4\pi} W_{pp'}^\ell. \quad (33)$$

Here we write the full window function matrix as $W_{pp'}^\ell$, and the usual ‘window function’ as $W_\ell = (1/N_p) \text{Tr}(W^\ell) = (1/N_p) \sum_p W_{pp'}^\ell$. The Fisher matrix for any other set of parameters can be recovered from that of the power spectrum by the appropriate Jacobian matrix:

$$F_{ii'} = \sum_{\ell\ell'} \frac{\partial C_\ell}{\partial b_i} F_{\ell\ell'} \frac{\partial C_{\ell'}}{\partial b_{i'}}. \quad (34)$$

Now we can determine the effect of a window function with an asymmetric beam on parameter errors. We refer all the requisite quantities to those with a symmetric beam. Define $W_{pp'}^\ell \sim r_\ell \bar{W}_{pp'}^\ell$, where $\bar{W}_{pp'}^\ell$ is the window function for a symmetric beam and $r_\ell \sim R(\ell)$ is an appropriate pixel average of the ratio R we defined in Eq. 23. Also define $S_{pp'} = a \bar{S}_{pp'}$ where again \bar{S} is the quantity for a symmetric beam, and a is thus a weighted average of the r_ℓ . Since the form of W will not be the same as that of \bar{W} , these ratios are of course only approximations. With these definitions we

write the Fisher matrix in terms of symmetric-beam quantities:

$$\begin{aligned} F_{\ell\ell'} &\sim \frac{1}{2} \text{Tr} \left[(a \bar{S} + N)^{-1} r_\ell \bar{W}^\ell (a \bar{S} + N)^{-1} r_{\ell'} \bar{W}^{\ell'} \right] \\ &= \frac{r_\ell r_{\ell'}}{a^2} \frac{1}{2} \text{Tr} \left[(\bar{S} + N/a)^{-1} \bar{W}^\ell (\bar{S} + N/a)^{-1} \bar{W}^{\ell'} \right] \\ &= \frac{r_\ell r_{\ell'}}{a^2} F_{\ell\ell'}(\bar{S}, N/a). \end{aligned} \quad (35)$$

That is, we can write the Fisher matrix as approximately a factor times the Fisher matrix for a symmetric beam, with the noise variance degraded by $1/a$. We might expect this factor, $r_\ell r_{\ell'}/a^2$, to be of order one.

In particular, for an experiment with uniform noise, we can write the Fisher matrix for an experiment observing a fraction f_{sky} of the sky with a symmetric beam B_ℓ as (approximately)

$$F_{\ell\ell'} \simeq (\ell + 1/2) f_{\text{sky}} \left[C_\ell + \frac{1}{\bar{w} B_\ell^2} \right]^{-2} \delta_{\ell\ell'}. \quad (36)$$

Here, $\bar{w} = \text{Tr}(N^{-1})$ is the total weight of the experiment, so the effect of the beam asymmetry is to make the replacement $\bar{w} \rightarrow a \bar{w}$; when the noise term dominates, the error on C_ℓ is increased by $1/a$.

3.4.2 Off-Diagonal Elements of the Window Function Matrix

We now assess the magnitude of the off-diagonal elements of the window function matrix in the presence of beam elongation due to small values of the parameter L . We will be interested in the ratio of Eq. 20, which is the general expression for the window function with an asymmetric beam, to Eq. 18, which assumes a symmetric beam

$$\begin{aligned} R_{tt'}(k) &= W_{tt'} / \{ B^2(k) J_0(kr_{tt'}) \} \\ &= \left[\frac{1}{J_0(kr_{tt'})} \right] \int \frac{d\theta_k}{2\pi} e^{-ikr_{tt'} \cos \theta_k} \\ &\quad \times [1 + (kv\tau)^2 \cos^2(\theta_k - \theta_t)]^{-1/2} \\ &\quad \times [1 + (kv\tau)^2 \cos^2(\theta_k - \theta_{t'})]^{-1/2}. \end{aligned} \quad (37)$$

Note that the original symmetric beam $B(k)$ drops out of this expression. When this ratio is small the beam elongation is having a large effect. While this ratio cannot be calculated analytically, we can gain much insight into the time-time correlations by considering the range in which $kv\tau = \ell/\ell_\tau$ is less than one. We then compute the integral numerically for larger values of $kv\tau$.

Expanding Eq. 20 in terms of $\alpha \equiv (kv\tau)^2$, redefining the zero point of the angular integral, and working to order α^2 we find

$$\begin{aligned} R_{tt'}(k) &= \frac{1}{J_0(kr_{tt'})} \int_0^{2\pi} \frac{d\theta}{2\pi} e^{ikr \sin \theta} \left\{ 1 \right. \\ &\quad - \frac{\alpha}{2} [\sin^2(\theta_t - \theta) + \sin^2(\theta_{t'} - \theta)] \\ &\quad + \alpha^2 \left[\frac{3}{8} \sin^4(\theta_t - \theta) \right. \\ &\quad + \alpha^2 \frac{1}{4} \sin^2(\theta_t - \theta) \sin^2(\theta_{t'} - \theta) \\ &\quad \left. \left. + \frac{3}{8} \sin^4(\theta_{t'} - \theta) \right] \right\}. \end{aligned} \quad (38)$$

By contour integration, this can be broken up into a sum of spherical Bessel functions:

$$\begin{aligned}
 R_{tt'} J_0(kr) &= J_0(kr) \\
 &- \frac{\alpha}{2} \left[J_0(kr) - \frac{\cos(2\theta_t) + \cos(2\theta_{t'})}{2} J_2(kr) \right] \\
 &+ \frac{\alpha^2}{32} \left\{ \left(\frac{3}{2} \cos^4 \theta_t + \cos^2 \theta_t \cos^2 \theta_{t'} + \frac{3}{2} \cos^4 \theta_{t'} \right) \right. \\
 &\quad \times [3J_0(kr) - 4J_2(kr) + J_4(kr)] \\
 &+ (9 \cos^2 \theta_t \sin^2 \theta_t + \cos^2 \theta_t \sin^2 \theta_{t'}) \\
 &\quad + 4 \cos \theta_t \sin \theta_t \cos \theta_{t'} \sin \theta_{t'} \\
 &\quad + \sin^2 \theta_t \cos^2 \theta_{t'} + 9 \cos^2 \theta_{t'} \sin^2 \theta_{t'}) \\
 &\quad \times [J_0(kr) - J_4(kr)] \\
 &+ \left. \left(\frac{3}{2} \sin^4 \theta_t + \sin^2 \theta_t \sin^2 \theta_{t'} + \frac{3}{2} \sin^4 \theta_{t'} \right) \right. \\
 &\quad \times [3J_0(kr) + 4J_2(kr) + J_4(kr)] \left. \right\}. \quad (39)
 \end{aligned}$$

We note that for $kr \gg 1$

$$J_l(x) \longrightarrow \frac{1}{x} \sin \left(x - \frac{l\pi}{2} \right), \quad (40)$$

and thus Eq. 39 becomes

$$\begin{aligned}
 R_{tt'} &= 1 - \frac{\alpha}{4} [2 + \cos(2\theta_t) + \cos(2\theta_{t'})] \\
 &+ \frac{\alpha^2}{8} (3 \cos^4 \theta_t + 2 \cos^2 \theta_t \cos^2 \theta_{t'} + 3 \cos^4 \theta_{t'}) \quad (41)
 \end{aligned}$$

We examine Eqs. 39 and 41 for three different configurations of asymmetric beams that are the interesting cases in the range of possible topologies. Fig. 3 shows the three configurations. In Case 1 the beams are separated along the direction of the scan. In Case 2 the beams are separated perpendicular to the scan, and in Case 3 the separation between the beams is parallel to the scan direction for one beam, and perpendicular for the other beam. For each one of these configurations we fix the distance scale r at two values, and plot in Figure 4 the behavior of $R_{tt'}$ as a function of k . We let k vary from $k = 0$ up to $k_{\max} = 1/(2v\tau)$ so that the approximation $\alpha < 1$ is valid throughout.

Case 1, shown in the upper left panel of Figure 4, is obtained by taking $\theta_t = \theta_{t'} = 0$ in Eq. 39. The periodic spikes in the value of $R_{tt'}$ are due to the slight shift between the zeros of Eq. 39 and $J_0(kr)$. Ignoring these spikes we observe the following properties of $R_{tt'}$. Near $k = 0$, i.e., for very long wavelengths, there is no difference whether the beams are elongated or not. As k increases $R_{tt'}$ decreases for both values of r indicating a smaller off-diagonal elements compared to the symmetric beam case. There is less attenuation for small r as compared to large r .

To understand this we note that only those \mathbf{k} vectors that are directed near the line between the two beams contribute to the angular average performed in Eq. 38. Since the asymmetric beams are most widened in that direction large k 's are effectively smeared (hence $R_{tt'} < 1$). Larger attenuation is obtained at large beam separation because a narrower range of wave vectors, and only those that are aligned in the beam elongation direction, contribute to the

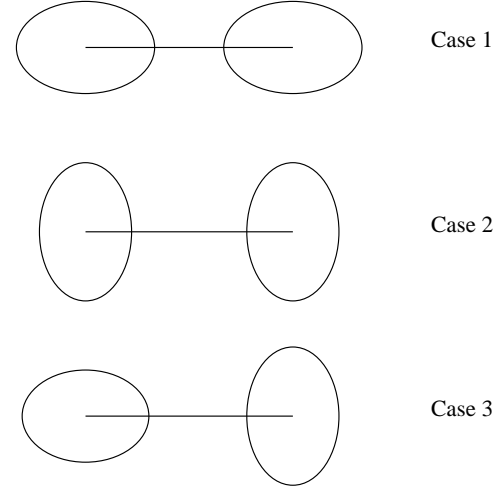


Figure 3. Three beam configurations that contribute to the off-diagonal elements of the window function matrix. The configurations shown span the range of interesting topologies.

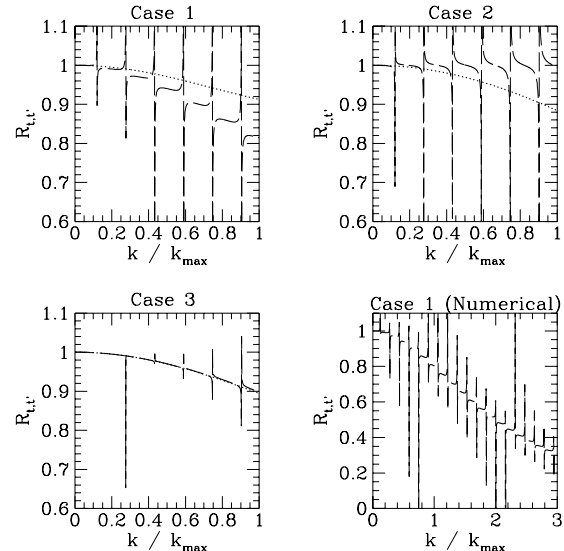


Figure 4. $R_{tt'}(k) = W_{tt'}/B^2(k)J_0(kr)$ for the three different topologies illustrated in Fig. 3. The upper left panel is Case 1, the upper right panel is Case 2, and the lower left panel is Case 3. In each panel $r = 1/k_{\max}$ (dotted) and $r = 20/k_{\max}$ (long dashed), where $k_{\max} = 1/(2v\tau)$. The periodic spikes are due to the shift between the zeros of Eq. 39 and $J_0(kr)$, and they can be ignored. Note that in these plots the vertical axis starts at $R_{tt'} = 0.6$. In the lower right panel we show Case 1 again for a larger span in k and for $r = 20/k_{\max}$. These results were obtained by numerically integrating Eq. 37. In the range of overlap in k the top left and bottom right panels agree.

angular average. Within this range of k 's the largest attenuation compared to the symmetric beam case is $\lesssim 20\%$. This limiting value is also obtained from Eq. 41 with $\theta_t = \theta_{t'} = 0$ which gives $R_{tt'} \approx 1 - \alpha + \alpha^2 = 0.8$.

Case 2 is obtained by taking $\theta_t = \theta_{t'} = \pi/2$ in Eq. 39. The upper right panel of Fig. 4 shows $R_{tt'}(k)$ for this case. Similar to Case 1, when $k = 0$ we obtain the symmetric beam case, $R_{tt'} = 1$. For $r = 20/k_{\max}$ there is no change in R as

k increases, and there is $\sim 10\%$ change for the $r = 1/k_{\max}$ case.

The physical explanation is similar to the reasoning in Case 1. The beams are narrowest in the direction of their separation. For large r only those k vectors that are aligned with the narrow dimension of the beam contribute to the angular average in Eq. 39. Hence there is effectively no difference between the symmetric beam case and the asymmetric case. The large r limit as obtained from Eq. 41 is $R_{tt'} = 1$. At small r values k vectors which are in the direction of the beam elongation contribute to the angular average. In this case $R_{tt'}$ is smaller compared to either the symmetric case or to the large r value.

Case 3 is obtained by taking $\theta_t = 0$ and $\theta_{t'} = \pi/2$ in Eq. 39. The lower left panel of Fig. 4 shows $R_{tt'}(k)$ for this case. For arguments similar to the ones in the previous cases we expect, and indeed observe, little difference between the two values of r . We also observe an overall attenuation at k_{\max} of $\sim 10\%$. This agrees with the asymptotic value for large r , $R_{tt'}(k) \approx 1 - \alpha/2 + 3/8\alpha^2 = 0.9$.

Within the approximation $k\tau = \ell/\ell_\tau \leq 0.5$ the largest reduction in the off-diagonal elements occurred for case 1, and for large values of r . For this case we continue the analysis for larger values of $k\tau$ by numerically integrating Eq. 37. The result of this numerical integration is shown in the lower right panel of Fig. 4. We find that the analytic approximation is excellent for $k\tau = \ell/\ell_\tau \leq 0.5$ and that when $\ell/\ell_\tau = 1$ the magnitude of these particular off-diagonal elements is about 50% of their values in the symmetric beam case.

We emphasize that we are considering here the effect of the asymmetric beam *relative* to the symmetric beam case. In Case 1 the asymmetric beam causes the greatest relative effect at large separation. However, the *absolute* contribution of these matrix elements to the signal at large ℓ will be small because large separations sample mainly small ℓ values (that is, the matrix elements are suppressed for $kr \simeq \ell r \gg 1$). We thus find that for the ℓ range where beam elongation is important, i.e., large ℓ , the matrix elements are not attenuated significantly compared to the symmetric beam case, certainly less than the 50% reduction observed for the most severe case at $\ell/\ell_\tau = 1$. Based on the arguments of Section 3.4.1 we expect a similar increase in the relative errors $\delta C_\ell/C_\ell$. The change in the relative error expected for any one of the cosmological parameters will be similar or smaller, and thus the major conclusions of Table 1 will not change.

4 DISCUSSION

Our point source response analysis shows that using a combination of bolometer time constant, scan speed, and beam size such that $L = \sigma/v\tau = \ell_\tau/\ell_\sigma \gtrsim 2.5$ results in relatively small increase in the effective beam size, less than 16%, and the spatial phase shift is less than 0.2σ . Because the window function encodes information from the nominal beam dimension as well as from the enlarged one the effect of a smaller L is less pronounced on the window function than it is on the point source response in the scan direction. In the Gaussian approximation the fractional effective increase in beam size derived from the window function analysis is a

factor of two smaller than that derived from the point source response (Eq. 28).

Our analysis of the performance of Planck-HFI indicates that choosing $L \sim 0.5$ will not be detrimental to the ability to extract cosmological parameters. This is a consequence of HFI's small beam size and high sensitivity. The HFI, with its nominal $\ell_\sigma = 1/\sigma$ which range from 725 to 1800, will determine the CMB power spectrum with high accuracy over a very broad range of ℓ . A degradation of its performance at high ℓ values does not diminish its capability significantly. It will generally be the case that the ability of any experiment with $\ell_\sigma \gtrsim 800$ to extract cosmological parameters will not be affected significantly with $L \gtrsim 0.5$, if the universe is any variant of the CDM model.

There are strong arguments for maintaining high resolution capability for a CMB experiment. We do *not* know that the universe is any variant of the cold dark matter model, or indeed that the fluctuations are Gaussian. High resolution will undoubtedly be important to test this latter assumption. Also, the ability to remove foregrounds and to detect point sources relies to some extent on high ℓ information and the ability to observe small-scale non-Gaussian structures.

If we are interested in achieving the maximum possible resolution, we wish to minimize a quantity like the effective 2-d beamwidth $\sigma_{2d}^2 \simeq \sigma^2(1 + L^{-2}/2)$. On the other hand, other considerations will make a *smaller* L more desirable. A fast scan speed increases the scale over which instrument noise is uncorrelated. Such broad temporal and/or angular scales can be used to better characterize the instrument's noise, to increase the ℓ range to which the experiment is sensitive, or for a better recovery of the underlying two dimensional sky signal (Tegmark 1997a). The form of σ_{2d} argues that we quickly reach a regime of diminishing returns as $L \gg 1$. For a given experiment the final determination of L depends on a global optimization which includes the expected instrument noise characteristics and the targeted science. Our analysis indicates that $1 \lesssim L \lesssim 2.5$ provides a range over which the small angular scale performance is not affected significantly, while allowing flexibility in tuning either the bolometer response time and/or the scan speed. For the HFI in particular, relaxing the value by a factor of ~ 2 , to $L \sim 1.5$, may increase the dynamic range over which the instrument and satellite parameters can be varied. Some experiments may choose to use even smaller values of L .

ACKNOWLEDGMENTS

We acknowledge and thank Viktor Hristov and Phil Mauskopf who first investigated the relation between the scan speed, beam size and detector response time. Phil Mauskopf has also independently suggested the use of the temporal window function. We thank Pedro Ferreira for discussions, and Paul Richards for comments on the manuscript. We are grateful to Dick Bond for the use of the code that calculates the errors on the determination of the cosmological parameters. S. H. and A. H. J. acknowledge support by NASA grant NAG5-3941 and by NSF cooperative agreement AST-9120005. S. H. was also supported by NASA grant NAG5-4454 and A. H. J. by NAG5-6552. E. S. is supported by an NSF graduate student fellowship.

REFERENCES

Bond J. R., Efstathiou G., Tegmark M., 1997, MNRAS, 291, L33.
Hristov V., 1994, private communication.
Jungman G., Kamionkowski M., Kosowsky A., Spergel D. N.,
1996, Phys. Rev. D, 54, 1332.
Richards P.L., 1994, J. Appl. Phys., 76, 1.
Tegmark M., 1997a, Phys. Rev. D, 56, 4514.
Tegmark M., 1997b, ApJ, 480, L87.
White M., 1997, private communication.
White M., Scott D., Silk J., 1994, ARA&A, 32, 319.
Wright E.L., astro-ph/9612006.
Zaldarriaga M., Spergel D. N., Seljak U., 1997, ApJ, 488, 1.